Emittance growth mechanisms for space-charge dominated beams in fixed field alternating gradient and proton driver rings

New Journal of Physics
The open-access journal for physics

Emittance growth mechanisms for space-charge dominated beams in fixed field alternating gradient and proton driver rings

S Y Lee[1,2,3], G Franchetti[2], I Hofmann[2], F Wang[1] and L Yang[1]

[1] Department of Physics, Indiana University, Bloomington, IN 47405, USA
[2] GSI, Darmstadt D64291, Germany
E-mail: shylee@indiana.edu

New Journal of Physics **8** (2006) 291
Received 30 May 2006
Published 28 November 2006
Online at http://www.njp.org/
doi:10.1088/1367-2630/8/11/291

Abstract. Systematic space-charge resonances are found to cause substantial emittance growth in proton driver rings and non-scaling fixed field alternating gradient (FFAG) accelerators. To avoid systematic nonlinear resonances, the phase advance of each cell must avoid $\pi/2$ and $\pi/3$. This limits the betatron tune range and the momentum acceptance for non-scaling FFAG accelerators. The emittance growth factor (EGF), defined as the ratio of final emittance to the initial emittance, is found to obey scaling properties in the linear space-charge tune shift parameter, the tune ramping rate, and stop-band widths of random quadrupole and skew-quadrupole errors.

[3] Author to whom any correspondence should be addressed.

PII: S1367-2630(06)25715-X

Contents

1. Introduction

Emittance evolution for space-charge dominated beams is one of many important topics in high intensity beam accelerators and storage rings. Even a small fraction of beam loss in these accelerators can cause radiation and operation problems. It is imperatively important to minimize beam loss and understand the emittance evolution.

There are many sources that can cause emittance growth. In linacs, the emittance growth can arise from the transverse–longitudinal (synchro-betatron) coupling, halo formation induced by collective envelope-modes or structure resonances, etc. In circular accelerators, candidates for emittance growth are the half-integer stop-band that can perturb the beam envelope function [1]–[3], the Montague resonance [4], and the sum resonance induced by the random skew-quadrupole field [5].

Because emittance growth is an important issue for high intensity beams, many numerical simulation codes have been constructed to study the emittance evolution [6]–[10]. These computer codes can study the interplay between space-charge force and other beam dynamics issues, such as dynamic ramping of the betatron tunes through betatron and synchrotron resonances, effect of beam acceleration in rf cavities located in dispersive region, etc.

Resonance crossing is an important subject in accelerator physics [11]. In particular, the betatron tunes of non-scaling fixed field alternating gradient (FFAG) accelerators may cross many resonances during the beam acceleration. There are a few studies on the effects of resonance crossing in the FFAG [12], which examine only non-systematic resonances, that are in principle correctable. This paper is intended to study the emittance growth mechanisms in high intensity accelerators during the stacking process and rapid cycling synchrotrons, such as FFAG accelerators. In particular, we will study the emittance growth mechanism resulting from the systematic space-charge force even when the FFAG accelerator is perfectly designed and constructed. We build a model to examine key ingredients in the emittance growth, and study the effects of random-quadrupole and skew-quadrupole errors.

This paper is organized as follows. Section 2 discusses the algorithm of our multi-particle simulation model. The space-charge force of our model is based on the potential derived from a Gaussian beam distribution, where the horizontal and vertical rms beam radii are updated in each revolution. Although there are a few self-consistent space-charge codes that can be used to study the emittance evolution, we choose the potential model in order to provide a fast parametric study. Section 3 studies the effect of systematic nonlinear space-charge resonances on emittance growth during the beam injection stacking. We also employ this particle tracking model to evaluate the effects of random errors in dipoles, quadrupoles, and skew-quadrupole fields on the beam emittances. Section 4 studies the effect of tune ramp through betatron resonances. We limit our study to the systematic nonlinear space-charge resonances, and linear resonances induced by quadrupole and skew-quadrupole errors. Section 5 presents conclusions and discussions.

2. Algorithm of multi-particle simulation with space-charge

To understand the phenomena involved in emittance growth, we construct a multi-particle code to study the emittance evolution. As the beam gets stacked in a synchrotron, particles experience a space-charge force proportional to the accumulated beam intensity. We track particle-motion in the presence of the space-charge force to extract the essential mechanisms of emittance growth. Our algorithm is given as follows.

2.1. Energy gain in rf cavities

The horizontal phase space coordinates are $x = x_\beta + D(\Delta E/\beta^2 E)$ and $x' = x'_\beta + D'(\Delta E/\beta^2 E)$, where (x_β, x'_β) are the betatron coordinates, and (D, D') are the dispersion functions. Since each particle gains the same amount of energy $\Delta E = u$ in an rf cavity, the changes of the betatron coordinates are $\Delta x_\beta = -Du/\beta^2 E$ and $\Delta x'_\beta = -D'u/\beta^2 E$. The beam centroid is constantly carrying out the coherent betatron motion, excited by the energy gain in cavities. The effect is more important at lower energies. The effective kick angles of these cavities are normally less than 1×10^{-5} rad; its effect is small unless all cavities are located in a single straight section [5]. We will not discuss this issue further in this paper.

2.2. FODO cells and random linear errors

We consider an accelerator lattice made of 24 FODO cells, where a FODO cell is made of a focusing quadrupole and a defocusing quadrupole separated by drift spaces or dipoles. Particle transport in each FODO cell is carried out by the transfer matrix from D to F, and F back to D with

$$M_{\mathrm{D}\to\mathrm{F}} = \begin{pmatrix} \sqrt{\dfrac{\beta_{x,\mathrm{F}}}{\beta_{x,\mathrm{D}}}}\cos\psi_x & \sqrt{\beta_{x,\mathrm{F}}\beta_{x,\mathrm{D}}}\sin\psi_x & 0 & 0 \\ -\dfrac{1}{\sqrt{\beta_{x,\mathrm{F}}\beta_{x,\mathrm{D}}}}\sin\psi_x & \sqrt{\dfrac{\beta_{x,\mathrm{D}}}{\beta_{x,\mathrm{F}}}}\cos\psi_x & 0 & 0 \\ 0 & 0 & \sqrt{\dfrac{\beta_{z,\mathrm{F}}}{\beta_{z,\mathrm{D}}}}\cos\psi_z & \sqrt{\beta_{z,\mathrm{F}}\beta_{z,\mathrm{D}}}\sin\psi_z \\ 0 & 0 & -\dfrac{1}{\sqrt{\beta_{z,\mathrm{F}}\beta_{z,\mathrm{D}}}}\sin\psi_z & \sqrt{\dfrac{\beta_{z,\mathrm{D}}}{\beta_{z,\mathrm{F}}}}\cos\psi_z \end{pmatrix},$$

$$M_{\mathrm{F}\to D} = \begin{pmatrix} \sqrt{\dfrac{\beta_{x,\mathrm{D}}}{\beta_{x,\mathrm{F}}}}\cos\psi_x & \sqrt{\beta_{x,\mathrm{F}}\beta_{x,\mathrm{D}}}\sin\psi_x & 0 & 0 \\ -\dfrac{1}{\sqrt{\beta_{x,\mathrm{F}}\beta_{x,\mathrm{D}}}}\sin\psi_x & \sqrt{\dfrac{\beta_{x,\mathrm{F}}}{\beta_{x,\mathrm{D}}}}\cos\psi_x & 0 & 0 \\ 0 & 0 & \sqrt{\dfrac{\beta_{z,\mathrm{D}}}{\beta_{z,\mathrm{F}}}}\cos\psi_z & \sqrt{\beta_{z,\mathrm{F}}\beta_{z,\mathrm{D}}}\sin\psi_z \\ 0 & 0 & -\dfrac{1}{\sqrt{\beta_{z,\mathrm{F}}\beta_{z,\mathrm{D}}}}\sin\psi_z & \sqrt{\dfrac{\beta_{z,\mathrm{F}}}{\beta_{z,\mathrm{D}}}}\cos\psi_z \end{pmatrix}$$

where $\psi_{x,z} = 2\pi\nu_{x,z}/48$ is the phase advance in a half cell, $\beta_{x/z,\mathrm{F/D}}$ are betatron amplitude functions at the centre of the focusing and de-focusing quadrupole locations with $\alpha_{x,\mathrm{F/D}} = 0$ and $\alpha_{z,\mathrm{F/D}} = 0$. The parameters for the betatron amplitude and dispersion functions depend on the size of the accelerator. In our numerical example, we choose $\beta_{x,\mathrm{D}} = 6.3\,\mathrm{m}$, $\beta_{z,\mathrm{D}} = 21.4\,\mathrm{m}$, $\beta_{x,\mathrm{F}} = 40\,\mathrm{m}$, $\beta_{z,\mathrm{F}} = 8.3\,\mathrm{m}$, $D_{x,\mathrm{D}} = 2.54\,\mathrm{m}$, and $D_{x,\mathrm{F}} = 4.5\,\mathrm{m}$. These parameters correspond to the values of the lattice betatron amplitude function of the Fermilab Booster. We may change the values of these betatron amplitude functions to vary the systematic space-charge resonance strengths.

Systematic sextupoles and small random dipole, quadrupole, and skew-quadrupole errors are introduced as kicks to each particle:

$$x'' + K_x(s)x = b_0(s) + b_1(s)x + a_1(s)z - \tfrac{1}{2}b_2(s)(x^2 - z^2), \tag{1}$$

$$z'' + K_z(s)z = -a_0(s) - b_1(s)z + a_1(s)x + b_2(s)xz. \tag{2}$$

The dipole components b_0 and a_0 are applied to each particle with a random seed to simulate the closed orbit mis-injection. The random quadrupole error is intended to create a half-integer stop-band in order to test the importance of the envelope dynamics and the half-integer stop-band on particle motion. The quadrupole component $b_1(s)$ is generated by a random seed with zero tune shift, i.e. $\oint \beta_x(s)b_1(s)\,\mathrm{d}s = 0$ and $\oint \beta_z(s)b_1(s)\,\mathrm{d}s = 0$. The random skew-quadrupoles take into account the quadrupole roll and the vertical closed orbit error in sextupoles. All random numbers are generated by random seeds with uniform distribution from -1 to $+1$. The magnitude of these random linear error fields are controlled by amplitudes A_{b0}, A_{a0}, A_{b1}, and A_{a1} respectively, and the amplitude of the rms errors are $1/\sqrt{3}$ of the corresponding amplitudes.

The sextupole component b_2 is inherent to all dipoles. They are introduced as a thin lens kick at the end of each half cell. The sextupole strengths depend on the magnet type and the ramping cycle. However, we find that their effect on emittance is small, unless systematic third order resonances are encountered, i.e. $3\nu_x = P$ and $\nu_x + 2\nu_z = P$. We have also include random sextupoles in our program. We find that their effects on emittances are small unless resonance conditions are encountered. Since we are mainly interested in the effect of the space-charge force, we neglect all sextupoles in this study.

2.3. Space-charge force

Since the emittance growth time is much shorter than the synchrotron period, we consider only 2D simulation with a frozen longitudinal phase space at the centre of the bunch $s = 0$. For

a Gaussian charge distribution: $\rho(x,z)=\frac{Ne}{2\pi\sigma_x\sigma_z}\exp(-\frac{x^2}{2\sigma_x^2}-\frac{z^2}{2\sigma_z^2})$, the transverse space-charge potential is [13]

$$V(x,z)=\frac{K_{\rm sc}}{2}\int_0^\infty \frac{-1+\exp\left\{-\dfrac{x^2}{2\sigma_x^2+t}-\dfrac{z^2}{2\sigma_z^2+t}\right\}}{\sqrt{(2\sigma_x^2+t)(2\sigma_z^2+t)}}\,{\rm d}t \approx -\frac{K_{\rm sc}}{2}\left\{\left(\frac{x^2}{\sigma_x(\sigma_x+\sigma_z)}+\frac{z^2}{\sigma_z(\sigma_x+\sigma_z)}\right)\right.$$
$$\left.-\frac{1}{4\sigma_x^2(\sigma_x+\sigma_z)^2}\left(\frac{2+R}{3}x^4+\frac{2}{R}x^2z^2+\frac{1+2R}{3R^3}z^4\right)+\cdots\right\}, \tag{3}$$

where the singularity at $x=z=0$ is removed by the addition of the -1 term in the numerator of the integrand, $R=\sigma_z/\sigma_x$ is the aspect ratio, $K_{\rm sc}=2Nr_0/(\beta^2\gamma^3)$, is the generalized space-charge perveance, σ_x and σ_z are the horizontal and vertical rms beam radii, N is number of protons per unit length, and $r_0=1.5347\times10^{-18}$ m is the classical proton radius. The horizontal rms beam radius is composed of both the betatron and off-momentum width contributions. For a beam with Gaussian distribution in the longitudinal phase space, we find $N=N_{\rm B}/(\sqrt{2\pi}\sigma_{\rm s})$, where $N_{\rm B}$ is the number of particles in a bunch and $\sigma_{\rm s}$ is the longitudinal rms bunch length.

In order to test many conditions, we carry out non-self-consistent multi-particle simulation based on the space-charge potential model, i.e. the space-charge force is modified by the rms radii, but remains in the Gaussian-potential form. Although the distribution function may become non-Gaussian, our space-charge kick remains in the Gaussian beam approximation. Each particle experiences a space-charge kick given by

$$\Delta x'=-\frac{\partial V}{\partial x}\ell\approx\frac{K_{\rm sc}\ell}{2}F_{x,{\rm sc}},\qquad \Delta z'=-\frac{\partial V}{\partial z}\ell\approx\frac{K_{\rm sc}\ell}{2}F_{z,{\rm sc}}, \tag{4}$$

$$F_{x,{\rm sc}}=\frac{2x}{\sigma_x(\sigma_x+\sigma_z)}\exp\left\{-\frac{x^2+z^2}{(\sigma_x+\sigma_z)^2}\right\}, \tag{5}$$

$$F_{z,{\rm sc}}=\frac{2z}{\sigma_z(\sigma_x+\sigma_z)}\exp\left\{-\frac{x^2+z^2}{(\sigma_x+\sigma_z)^2}\right\}, \tag{6}$$

where ℓ is the length of the half cell. The form factors $F_{x,{\rm sc}}$ and $F_{z,{\rm sc}}$ in equation (4) are obtained by using the space-charge potential of equation (3) up to the second order expansion in round beam geometry, and exponentiated to produce *zero tune shift for large amplitude particles*.[4] Note that the approximation underestimates the space-charge kicks at $(x,z)>2(\sigma_x,\sigma_z)$. We compare the approximated form factor with the exact form factor derived from the space-charge potential in the appendix. Since we study the physics of emittance growth less than a factor of four, our

[4] Note that the space-charge kicks in equation (4) cannot be derived from a potential, and thus the resulting Montague resonance is only approximately correct. Since this paper focuses on other resonances, the approximation used here is justified. In the future, these space-charge kicks will be replaced by more time-consuming calculations with the complex error function.

model should be a reasonable approximation. The linear (Laslett) space-charge tune shifts are

$$\Delta\nu_{x,\mathrm{sc}} = \frac{1}{4\pi}\oint \frac{\beta_x(s)K_{\mathrm{sc}}}{\sigma_x(\sigma_x+\sigma_z)}\,\mathrm{d}s, \qquad \Delta\nu_{z,\mathrm{sc}} = \frac{1}{4\pi}\oint \frac{\beta_z(s)K_{\mathrm{sc}}}{\sigma_z(\sigma_x+\sigma_z)}\,\mathrm{d}s. \tag{7}$$

We will use $\Delta\nu_{\mathrm{sc0}}$ to represent either the horizontal or vertical space-charge tune shift parameter at the initial emittances. The space-charge force is approximated by 48 localized space-charge kicks per revolution. The rms beam radii calculated from the multi-particle phase space distribution is used for space-charge kicks in the next revolution. The advantage of this approximation is that the noise in the calculation of the rms radii is smoothed out in one revolution. The resulting calculation depends less on the number of macro-particles in the simulation. The disadvantage is that the variation of the rms radii resulting from the random quadrupole field error is washed out. The random quadrupole error can create beta-beat and beam size variation in the accelerator, and thus the space-charge force should also have the beta-beat frequency. The effect of the beta-beat in the space-charge force vanishes when we use the averaged rms beam radii from the previous revolution for the space-charge kick of the entire next revolution.

3. Emittances in high power neutron sources

We now explore the effect of systematic space-charge higher order resonances on the beam emittances. Some of these resonances are $4\nu_x = P, 4\nu_z = P, 2\nu_x + 2\nu_x = P, 6\nu_x = P$, etc. When the 4th order systematic space-charge resonance is encountered, each basic lattice cell has a phase advance of $\pi/2$. In actual high power neutron sources, we have $\Delta\nu_{\mathrm{sc0}} \approx 0.1 \sim 0.2$. Since we are studying the effect of the systematic space-charge resonances, we will artificially increase $\Delta\nu_{\mathrm{sc0}}$ to as large as 1.1.

3.1. Systematic space-charge resonances

When the accelerator is free from random errors, only systematic machine resonances can affect the beam performance. In our model of $P = 24$, the systematic 4th order space-charge resonances occur $4\nu_x = 24$, $4\nu_z = 24$, and $2\nu_x + 2\nu_z = 24$. Existence of the systematic 4th order space-charge resonance islands has been shown to exist in the self-consistent space-charge model calculations in the bunch rotation manipulation [14]. Experimental measurements of beam profiles at the KEK PS have also inferred that the large emittance growth has resulted from the systematic 4th order space-charge resonance [15].

We consider the case of high intensity beam with the initial rms emittances $\epsilon_{x0,\mathrm{rms}} = \epsilon_{z0,\mathrm{rms}} = 25\pi$ mm mrad and bare machine tunes located at $\nu_{x0} = 6.23$ and $\nu_{z0} = 6.2$. The beam is accumulated for 1000 injection turns reaching at the end $\Delta\nu_{\mathrm{sc0}} = 1.1$. In an actual high power neutron source, the $\Delta\nu_{\mathrm{sc0}}$ is only 0.2, and the beam never encounters the condition in our numerical simulation; however in a bunch compression process a tune shift of magnitude one is possible.

As the beam is injected into the accelerator, the betatron tunes for zero amplitude particles are pushed downward as shown on the top-left plot of figure 1. Note that the emittances begin to increase when the betatron tunes are pushed through the systematic resonances shown in the bottom left plot. The right plots of figure 1 show the normalized Poincaré maps at the end of a 1000 turn accumulation.

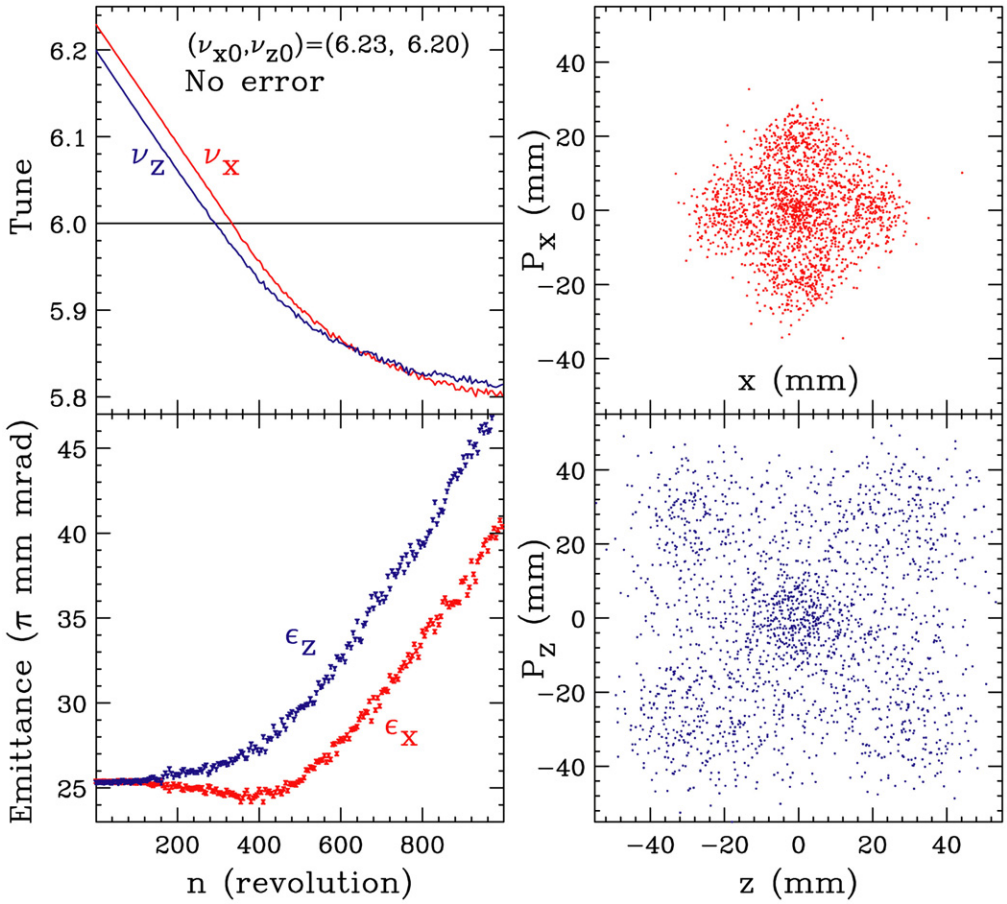

Figure 1. Top left plot: betatron tunes of the small amplitude particles as a function of injection revolution. When the tunes cross the systematic space-charge resonances, the emittances begin to increase, as shown on the bottom-left plot. Right plot: the normalized Poincaré surface of section at the end of 1000 revolution, showing the effect of the 4th order nonlinear space-charge resonance at $4\nu_x = P$ and $4\nu_z = P$, where $P = 24$ in our numerical example.

3.1.1. Stop-band widths of the 4th order resonances. The 4th order space-charge potential is

$$V_{\mathrm{sc},4}(x, z) = +\frac{K_{\mathrm{sc}}}{8\sigma_x^2(\sigma_x+\sigma_z)^2}\left(\frac{2+R}{3}x^4 + \frac{2}{R}x^2z^2 + \frac{1+2R}{3R^3}z^4\right). \tag{8}$$

We carry out a Floquet transformation and expand the space-charge potential in Fourier harmonics to obtain

$$\begin{aligned} V_{sc,4}(J_x, J_z, \psi_x, \psi_z, \theta) \approx & -\sum |G_{4,0,\ell}| J_x^2 \cos(4\psi_x - \ell\theta + \chi_{4,0,\ell}) \\ & -\sum |G_{0,4,\ell}| J_z^2 \cos(4\psi_z - \ell\theta + \chi_{0,4,\ell}) \\ & -\sum |G_{2,2,\ell}| J_x J_z \cos(2\psi_x + 2\psi_z - \ell\theta + \chi_{2,2,\ell}) \\ & -\sum |G_{2,-2,\ell}| J_x J_z \cos(2\psi_x - 2\psi_z - \ell\theta + \chi_{2,-2,\ell}), \end{aligned} \tag{9}$$

where $|G_{m,n,\ell}|$ and $\chi_{m,n,\ell}$ are the amplitude and phase of the resonance strength:

$$G_{4,0,\ell} = \frac{1}{96\pi} \oint \frac{K_{\rm sc}\beta_x^2(2\sigma_x+\sigma_z)}{\sigma_x^3(\sigma_x+\sigma_z)^2} \exp\{j(4\phi_x - 4\nu_x\theta + \ell\theta)\}\,{\rm d}s, \tag{10}$$

$$G_{0,4,\ell} = \frac{1}{96\pi} \oint \frac{K_{\rm sc}\beta_z^2(\sigma_x+2\sigma_z)}{\sigma_z^3(\sigma_x+\sigma_z)^2} \exp\{j(4\phi_z - 4\nu_z\theta + \ell\theta)\}\,{\rm d}s, \tag{11}$$

$$G_{2,2,\ell} = \frac{1}{16\pi} \oint \frac{K_{\rm sc}\beta_x\beta_z}{\sigma_x\sigma_z(\sigma_x+\sigma_z)^2} \exp\{j(2\phi_x + 2\phi_z - 2\nu_x\theta - 2\nu_z\theta + \ell\theta)\}\,{\rm d}s, \tag{12}$$

$$G_{2,-2,\ell} = \frac{1}{16\pi} \oint \frac{K_{\rm sc}\beta_x\beta_z}{\sigma_x\sigma_z(\sigma_x+\sigma_z)^2} \exp\{j(2\phi_x - 2\phi_z - 2\nu_x\theta + 2\nu_z\theta + \ell\theta)\}\,{\rm d}s. \tag{13}$$

Here β_x and β_z are the betatron amplitude functions, ν_x and ν_z are the betatron tunes, $\theta = 2\pi s/C$ is the orbital angle, C is the circumference of the accelerator, and the betatron phase advance functions are $\phi_x = \int_0^s {\rm d}s/\beta_x$, $\phi_z = \int_0^s {\rm d}s\beta_z$.

The resonance strengths for a beam with equal emittances $\epsilon = \epsilon_x = \epsilon_z$ can be factorized as:

$$G_{4,0,\ell} = g_{4,0,\ell}\frac{K_{\rm sc}C}{8\pi\epsilon^2}, \qquad G_{0,4,\ell} = g_{0,4,\ell}\frac{K_{\rm sc}C}{8\pi\epsilon^2},$$

$$G_{2,2,\ell} = g_{2,2,\ell}\frac{K_{\rm sc}C}{8\pi\epsilon^2}, \qquad G_{2,-2,\ell} = g_{2,-2,\ell}\frac{K_{\rm sc}C}{8\pi\epsilon^2},$$

where C is the circumference. The factor $K_{\rm sc}C/(8\pi\epsilon)$ is the linear Laslett space-charge tune shift in the round beam geometry, and the reduced resonance strength $g_{m,n,\ell}$ depends solely on the geometric factor of beam size modulation in each cell. For a lattice made of FODO cells at equal tunes, the reduced resonance strength are $g_{4,0,\ell} = 0.0148$, $g_{0,4,\ell} = -0.0149$, $g_{2,2,\ell} = -0.000104$, and $g_{2,-2,\ell} = 0.117$. The coefficients in our model calculation are approximated by two space-charge kicks in each FODO cell. Including the momentum width, these coefficients are about 0.0402, −0.0404, −0.00576, and 0.0982 for the Fermilab Booster parameters. However, we can change the betatron amplitude functions to vary the stop-band width. The SIS18 lattice at GSI is made of $P = 12$ triplet cells with the vertical betatron tune of 3.23. The variation of the betatron amplitude functions is smaller in a triplet cell, and the amplitudes of the reduced resonance strengths are 0.00125, −0.00133, 0.000262, and 0.124 respectively.

We observe that (i) $g_{0,4,\ell}$ and $g_{4,0,\ell}$ are out of phase and thus the phase space maps shown on the right plots of figure 1 are 45° from each other; (ii) the strength $G_{2,2,\ell}$ of the sum resonance for accelerator lattices is small, because the integrand of equation (12) is nearly constant and the Fourier amplitude of a constant at a nonzero harmonic is zero; and (iii) the Montague resonance strength is uniformly large for all accelerators. Although we have used only two space-charge kicks per FODO cell in numerical simulations, the resulting resonance strengths can be varied by changing the betatron amplitude functions at these space-charge kick locations.

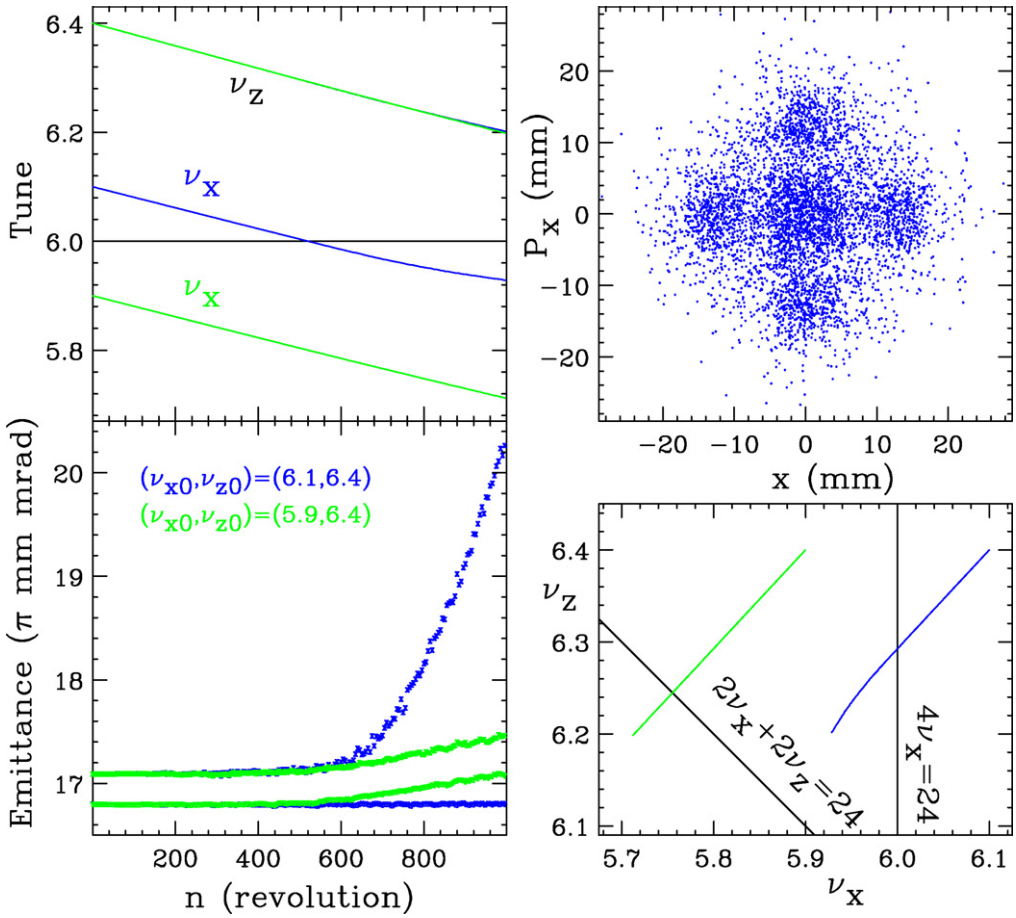

Figure 2. Beams with $(\nu_{x0}, \nu_{z0}) = (6.1, 6.4)$ (blue curves) and (5.9, 6.4) (green curves) are prepared to explore the effect of $4\nu_x$ and $2\nu_x + 2\nu_z$ resonances. Top left plot: the betatron tunes of small amplitude particles versus the injection turn. Bottom left plot: emittances versus the injection turn. Top right plot: Phase space map (x, P_x) at the end of beam accumulation for the case with bare tunes (6.1, 6.4). Bottom right plot: the tunes versus the resonance lines for both cases.

3.1.2. Space-charge sum resonance. To verify the smallness of the sum resonance strength, we use a beam with $\Delta\nu_{sc0} = 0.2$ in 1000 injection turns to explore $4\nu_x = 24$ and $2\nu_x + 2\nu_z = 24$ resonances. The blue curves in the left-hand side plots of figure 2 show the case with bare tunes at $(\nu_{x0}, \nu_{z0}) = (6.10, 6.40)$. As the injection turn increases, the horizontal tune crosses the $4\nu_x = 24$ resonance, and the horizontal emittance begins to increase. The top-right plot shows the normalized Poincaré map of the horizontal plane. The vertical emittance remains unchanged. The green curves in the left plots of figure 2 show the case with the bare tunes at $(\nu_{x0}, \nu_{z0}) = (5.90, 6.40)$. As the injection turn increases, the tunes cross the $2\nu_x + 2\nu_z = 24$ resonance, and both the horizontal and vertical emittances increase at a much lower rate.

3.2. Effects of linear errors

3.2.1. Half-integer stop bands. The quadrupole field errors can drive envelope resonance instability and coherent betatron motion. The envelope instability causes mis-matched β-function, and induces emittance growth. On the other hand, the quadrupole field error can also cause unstable betatron motion for each particle. The action of the particle will grow until $|\nu - \frac{p}{2}| > |J_{\rm p}|/2$, where ν is the betatron tune, p is an integer and $J_{\rm p}$ is the half-integer stop-band width:

$$J_{\rm p} = \frac{1}{2\pi} \oint \beta(s) \Delta K(s)\, {\rm e}^{-{\rm i}p\phi(s)}\, {\rm d}s. \tag{14}$$

Here $\beta(s)$ is either the horizontal or vertical betatron amplitude function, $\Delta K(s)$ is the quadrupole field error, $\phi(s) = \frac{1}{\nu}\int_0^s ({\rm d}s/\beta(s))$ is the corresponding normalized betatron phase, and s is the longitudinal coordinate. When the betatron tune ν of a particle sits at $p/2$, the action of the particle will grow exponentially as $\exp(2\pi|J_{\rm p}|n)$ where n is the revolution number [2].

We prepare a beam with $\Delta\nu_{\rm sc0} = 0.109$ and an initial rms emittance of 8.5π mm mrad, near the half integer stop-band at $\nu_{x0} = 6.5$. The random quadrupole-field errors has a stop-band width of $|J_{13}| = 5.46 \times 10^{-3}$ at $\nu_{x0} = 6.5$. Consider the following three cases: (i) a beam with 100 turn injection at a bare horizontal tune of $\nu_{x0} = 6.65$, and then ν_{x0} is ramped from 6.65 to 6.52 from 200 to 1200 revolutions; (ii) a beam with one turn injection at a fixed $\nu_{x0} = 6.52$; and (iii) a beam with 1000 turn injection at a fixed tune of 6.52. The top-left plots of figure 3 show the evolution of the small amplitude horizontal betatron tunes. The bottom-left plot shows the horizontal emittances. The black curve corresponds to case (i), red curve for case (ii), and blue curve for case (iii) respectively. The right plots shows the corresponding normalized phase space Poincaré maps at the end of 2000 revolutions.

The envelope mismatch is supposed to be the largest for the case (ii); however, it has the smallest emittance growth (see red curve in figure 3). The reason is that few particles fall within the stop-band width. If the betatron tunes of small amplitude particles were ramped through the half integer stop-band, emittance growth would occur. For both cases (i) and (iii), particles at the centre of the distribution are swept through the half-integer stop-band, and the emittance growth becomes inevitable. The phase space distributions, shown on the top and bottom plots of figure 3, reflect the nonlinear Mathieu instability in many dynamical systems (see e.g. [16]). Thus the essential emittance growth mechanism is the half-integer resonance due to the random quadrupole error.

3.2.2. All linear errors. The systematic 4th order space-charge resonances occur at $4\nu_x = P$ and $4\nu_z = P$, where the phase advance of each (FODO) cell is $\pi/2$. What happens if other linear errors are included? Figure 4 shows the emittance growth during the 1000-turn injection for the case of (i) no error (green curves), i.e. only space-charge resonances; (ii) with dipole field errors (blue curves) at $A_{b0} = 2.0 \times 10^{-5}$ rad and $A_{a0} = 7.5 \times 10^{-5}$ rad; (iii) with dipole field and quadrupole field errors (magenta curves) at $A_{b1} = 4.0 \times 10^{-4}\,{\rm m}^{-1}$; (iv) with additional skew-quadrupole error at $A_{a1} = 40 \times 10^{-3}\,{\rm m}^{-1}$ (red curves); and (v) with an additional systematic sextupole fields (black curves). The magnitudes of these random errors are the typically tolerance of accelerator magnets. The emittance growth from the systematic 4th order space-charge resonance dominates.

What happen if the betatron tunes do not encounter the systematic 4th order space-charge resonances? We set the bare betatron tunes at $(\nu_{x0}, \nu_{z0}) = (5.83, 5.80)$, i.e. the space-charge

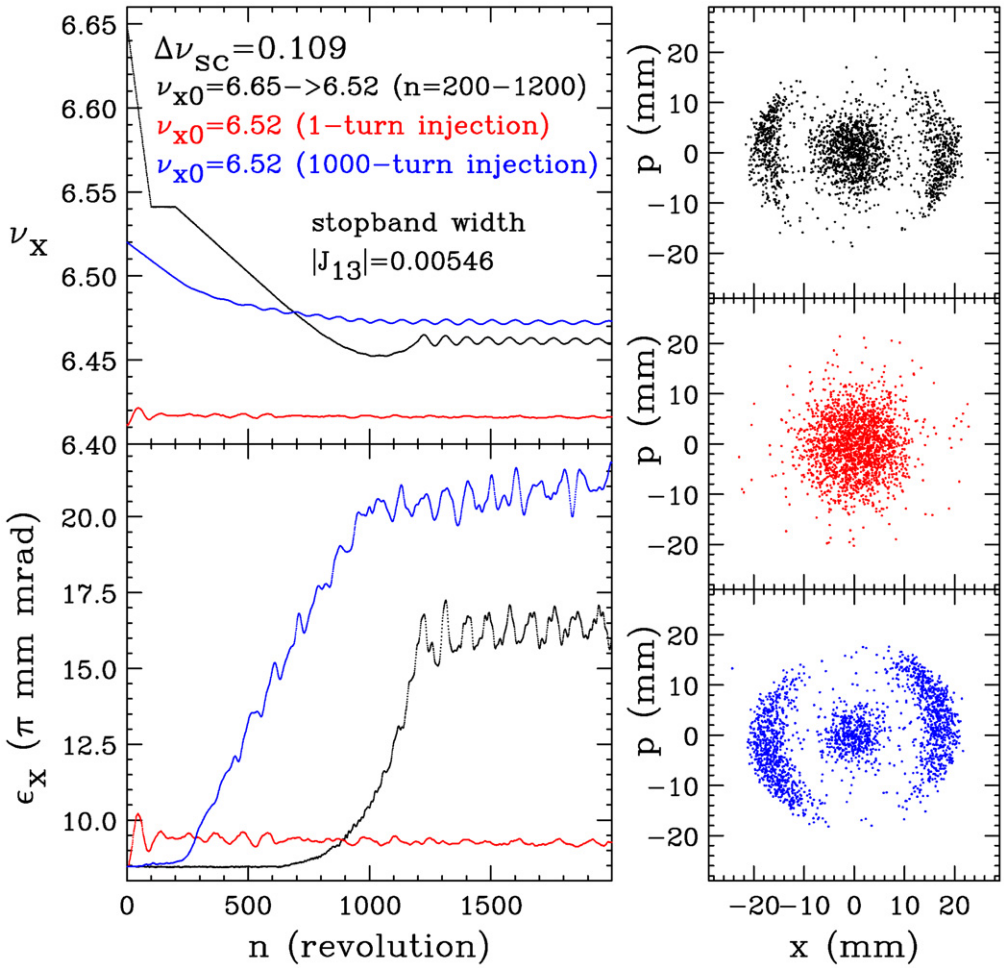

Figure 3. Effect of quadrupole error on emittance with $|J_p| = 5.46 \times 10^{-3}$ at $\nu_x = 6.5$ and $\Delta\nu_{sc0} = 0.109$. Left-hand side plots show tunes and emittances. Right-hand side plots show the normalized phase space maps at the end of 2000 revolutions. The black curve represents 100 turn injection at $\nu_{x0} = 6.65$ and ramped from 6.65 to 6.52 from 200 to 1200 revolutions. The red curve represents one turn injection at $\nu_{x0} = 6.52$. The blue curve is 1000 turn injection at $\nu_{x0} = 6.52$.

detuning does not cross any systematic space-charge resonances. The green curves of figure 5 show clearly that there is no emittance growth during the 1000-turn injection process (see green points), where a small emittance exchange is visible arising from the Montague resonance. However, when linear errors are included, similar to those of figure 4, the emittance increase becomes evident. The emittance growth arisely mainly from the sum resonance due to the random skew-quadrupoles. Although the resulting emittance growth is smaller than that of figure 4, the emittance increase is still sizable. The amount of emittance growth depends on the stop-band widths of quadrupole and skew-quadrupole errors. These stop-bands can in principle be corrected.

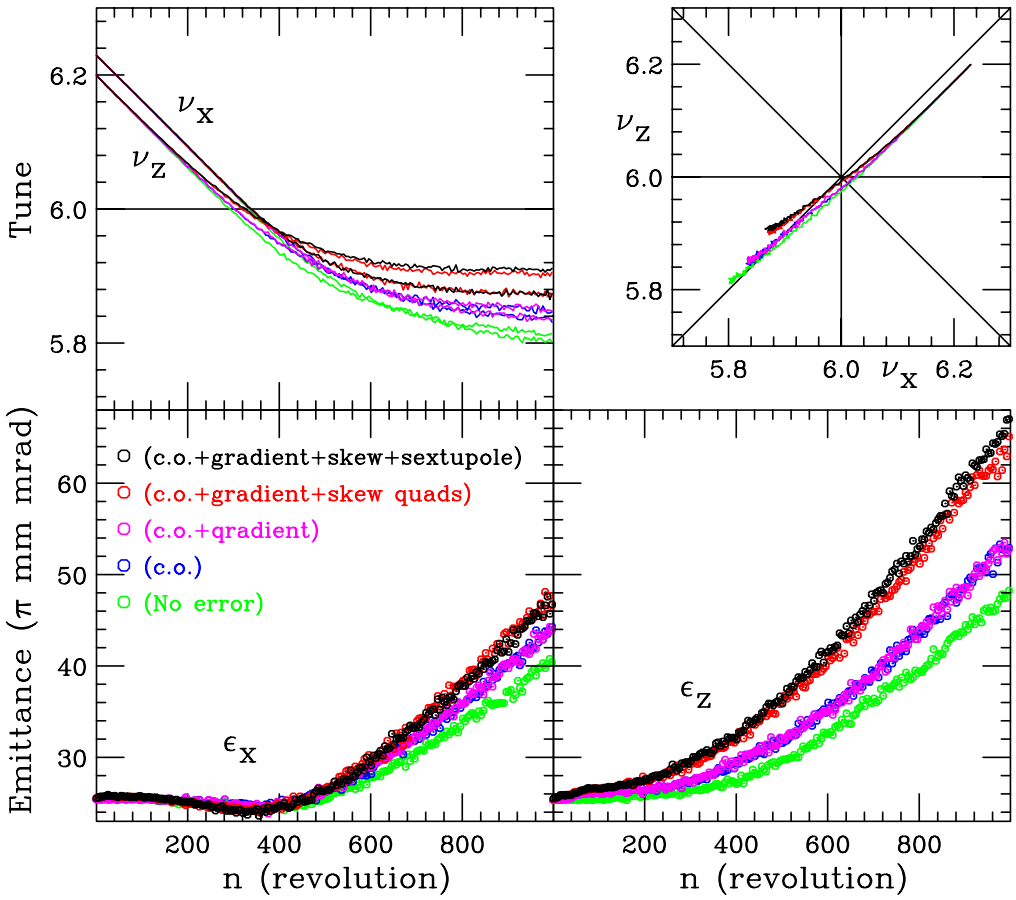

Figure 4. Tune and emittance evolution including various linear errors for the bare betatron tunes $(\nu_{x0}, \nu_{z0}) = (6.23, 6.20)$ with space-charge tune shift of 0.64 for small amplitude particles.

3.3. Higher order systematic space-charge resonances

Since the space-charge potential is highly nonlinear, higher order space-charge resonances can also be important. For this purpose, we set the bare tunes at $(\nu_{x0}, \nu_{z0}) = (4.25, 4.20)$. Similar to the 4th order systematic space-charge resonances, the betatron tunes for the small amplitude particles will decrease. When the tunes of a particle reach the resonance $6\nu_{x,z} = P$, the phase space coordinates of the particle experience coherent space-charge kicks. Eventually, the phase space distribution of the beam will evolve into resonance structure shown in the right-hand side plots of figure 6. Comparing with the emittance growth from the 4th order space-charge resonance shown in figure 1, we find that the emittance growth for the 6th order space-charge resonance is also important, shown in the bottom-left plot of figure 6.

Besides the 6th order space-charge resonances, the systematic 8th order space-charge resonances $8\nu_{x/z} = 2P$ can occur at the same tune as those of the 4th order resonance. The strength of the systematic 8th order resonance is the second harmonic Fourier integral of envelope shape functions. Unless the 4th order resonance is completely suppressed, the 8th order resonance is hardly visible in all calculations.

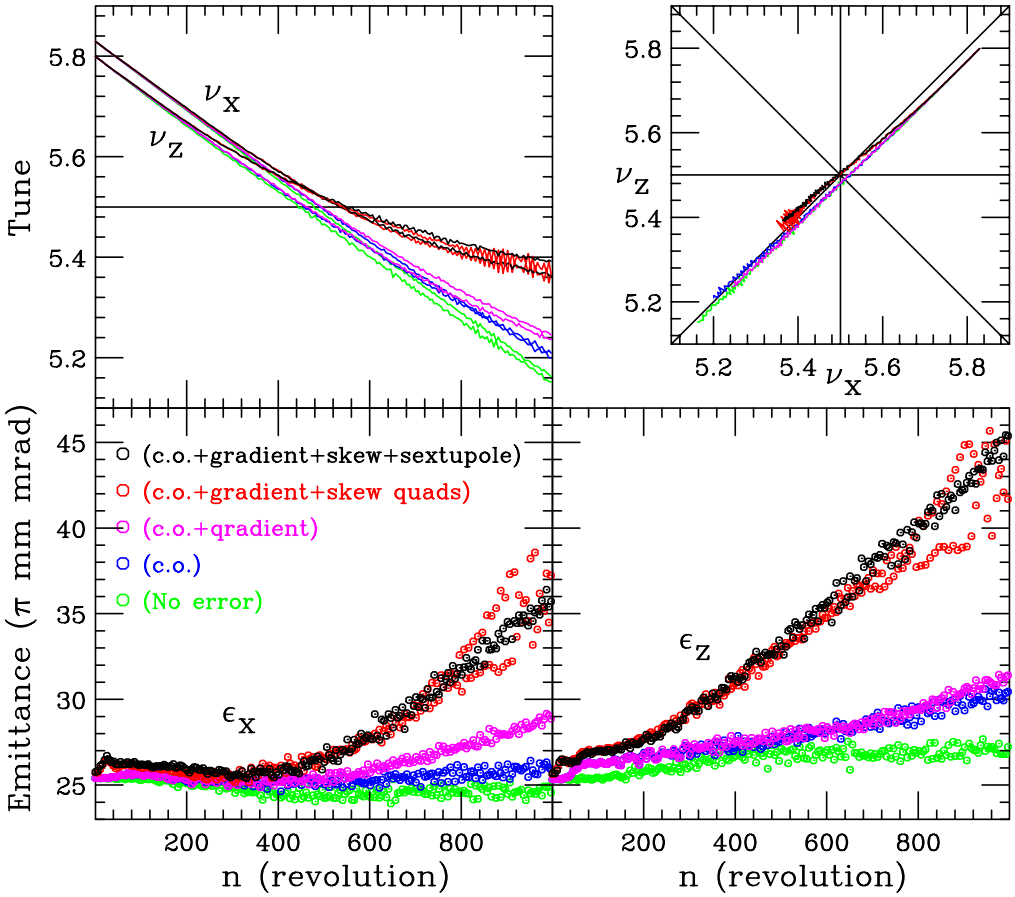

Figure 5. Similar to those of figure 4 except that the bare tunes $(\nu_{x0}, \nu_{z0}) = (5.83, 5.80)$ are chosen to avoid the 4th order systematic space-charge resonance.

4. Effect of tune ramp through resonances

There is a recent revival of interests in using the FFAG accelerators for proton drivers [17], which may find applications in muon colliders, neutrino factory, neutron sources, energy amplifiers, etc. The FFAG research in the United States focuses on a non-scaling design that requires a much smaller magnet aperture [18]. Unfortunately, the betatron tunes of the non-scaling FFAG cannot be maintained at a value within two integers. The betatron tunes decrease because the focusing field is kept nearly constant, while the beam momentum increases.

The FFAG accelerator may encounter many technical challenges in rf, magnet and vacuum technologies. However, its difficulties in beam physics have not been challenged. Emittance blowup for space-charge-dominated beams is one of many important topics in all high intensity accelerator and storage rings. For an FFAG accelerator, the betatron tune ramp rate is given by

$$\frac{\mathrm{d}\nu}{\mathrm{d}N} \approx -\nu\frac{\Delta E}{\beta^2 E}, \tag{15}$$

where ΔE is the energy gain in one revolution. Assuming that the energy gain per revolution is 1 MeV, we find that the tune ramp rate will be less than 0.02, i.e. the tune is changed by one

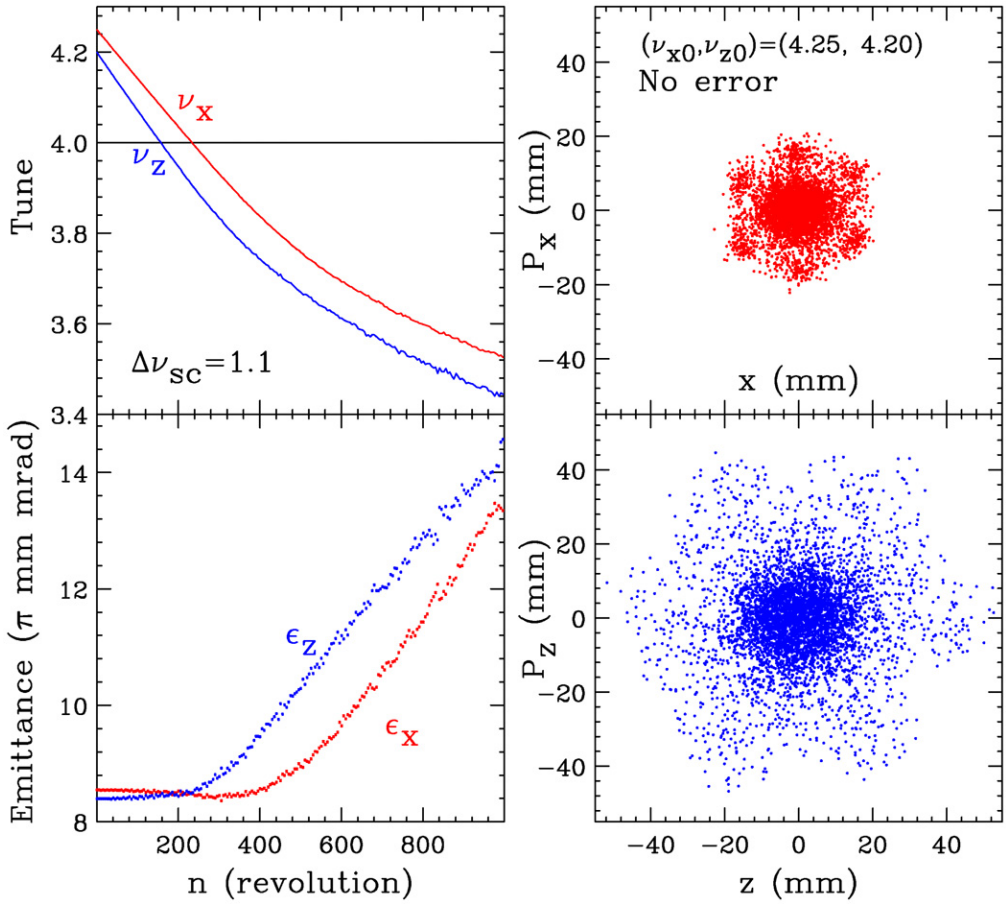

Figure 6. The bare tunes are set at $(\nu_{x0}, \nu_{z0}) = (4.25, 4.20)$ with 1000 turn injection at $\Delta\nu_{sc0} = 1.1$ to explore the 6th order systematic space-charge resonances. There is no random error in this calculation.

unit in 50 revolutions; however, for the sake of generality, we study the emittance evolution with $d\nu/dN$ from 0.001 to 0.05 to cover all possible tune ramp conditions.

We consider a beam intensity of 100 injection turns such that the total space-charge tune shift is about 0.15 and an initial rms beam emittance of 8.5π mm mrad in a perfectly designed and constructed accelerator without random errors. First, we consider the case of ramping the bare betatron tunes (ν_{x0}, ν_{z0}) from (6.25, 6.20) to (5.85, 5.80) linearly from 200 to 1000 revolutions, shown as blue curves in figure 7. Similarly, the case of the bare tunes ramping from (5.85, 5.80) to (6.25, 6.20) is shown as red curves in figure 7.

The emittance growth is very severe for the down-ramp, because the betatron tunes tend to stay longer at resonance as the emittances increase. When the betatron tunes approach the $4\nu_x = 24$ and $4\nu_z = 24$ resonances, particles are transported and trapped on to the 4th order resonance islands. After passing through the 4th order resonance, particles decohere into a ring in the phase space, shown in the right plots of figure 7. Since the up-ramp gives a faster crossing rate, the resulting emittance growth is much smaller [19]. Ramping through non-systematic resonance integers does not cause any emittance growth shown as the green curve in figure 7.

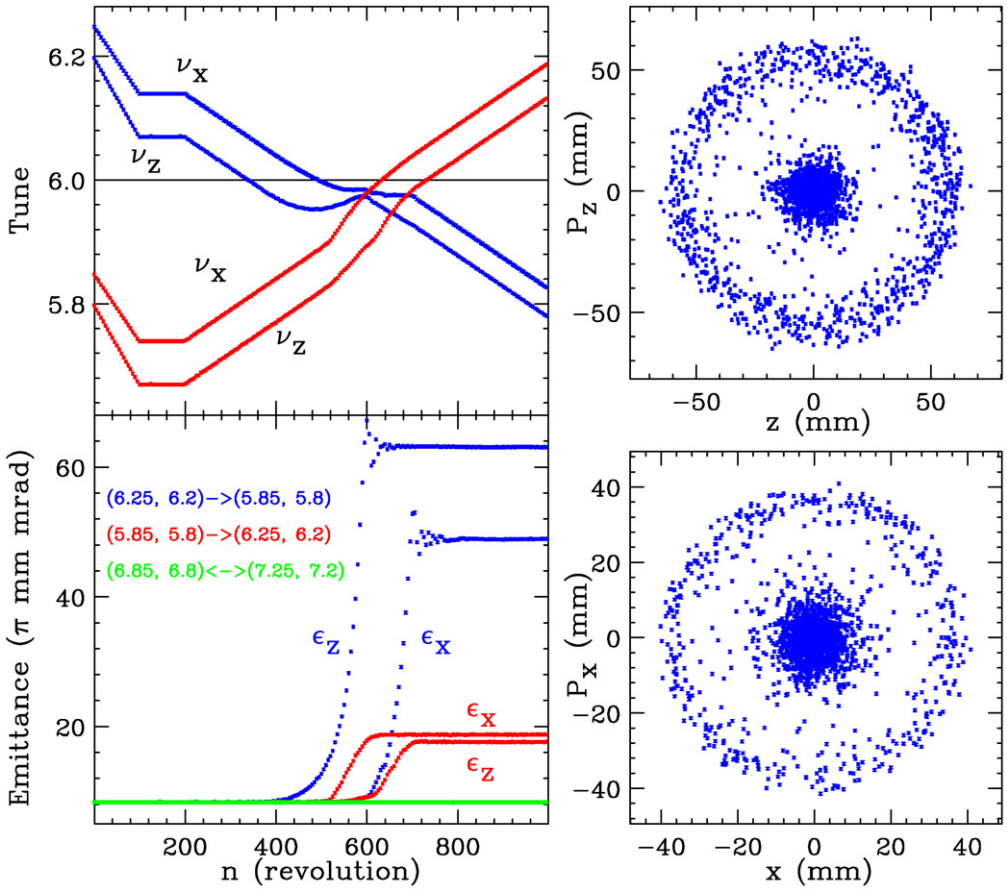

Figure 7. Left-hand side plots: betatron tunes and the normalized emittances. Effect of ramping betatron tunes through systematic space-charge nonlinear resonances. The blue curves corresponds to the down-ramp from $(\nu_{x0}, \nu_{z0}) = (6.25, 6.20)$ to (5.85, 5.80). Right-hand side plots: normalized phase space maps at the end of ramping in the down-ramp condition. The red curves corresponds to up-ramp condition from (5.85, 5.80) to (6.25, 6.20). The green curve correspond to ramping through integer tune without systematic space-charge resonance, i.e. from (6.85, 6.80) to (7.25, 7.20).

To quantify the emittance growth, we define the emittance growth factor (EGF) as the ratio of the final emittance to the initial one. We carry out calculations of EGF for the 4th order nonlinear space-charge resonances. The bottom plot of figure 8 shows the EGF as a function of resonance crossing rate: $\Delta\nu/\Delta n$, which is defined as the tune ramp per revolution. Note that the EGF shows a power law, i.e. the EGF is proportional to $(\Delta\nu/\Delta n)^{-0.62}$ in the low crossing rate regime.

The EGF depends also on the strength of the space-charge force. Using the linear space-charge tune shift parameter, $\Delta\nu_{sc0}$, as the scaling parameter, we find that the EGF almost increases linearly with $\Delta\nu_{sc0}$, as shown in the top plot of figure 8.

In fact, the EGF depends on the 4th order space-charge resonance strength. By varying the betatron function at the space-charge kick locations, we vary the resonance strength $g_{4,0,\ell}$ and $g_{0,4,\ell}$.

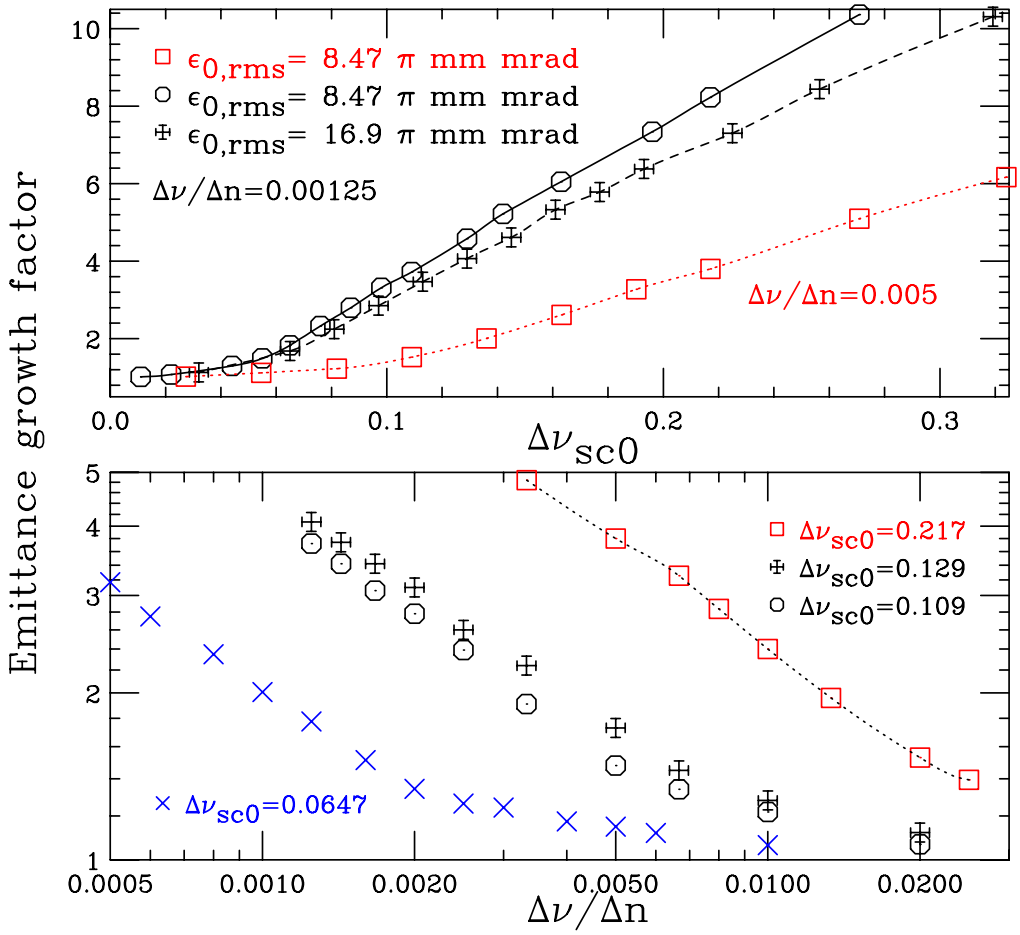

Figure 8. Bottom plot: the EGF, defined as the ratio of the final emittance to the initial emittance, is shown as a function of the resonance crossing rate, $\Delta\nu/\Delta n$, defined as the tune change per revolution. Top plot: The EGF versus $\Delta\nu_{sc0}$.

Figure 9 shows the EGF versus the tune ramp rate $d\nu/dN$ for various $g_{0,4,\ell}$. The X-symbols (green curve) correspond to the EGF obtained from a self-consistent space-charge calculations for the SIS18 by using the MICROMAP [7]. Since the self consistent space-charge calculation has an aperture limit, the turn-over of the EGF factor larger than four arises from beam loss. However, it is comforting to know that a self-consistent calculation gives a similar EGF scaling law!

The EGF has scaling properties EGF $\sim (d\nu/dN)^{-a}$, where a ranges from 0.60 to 0.80. Each EGF curve corresponds to a fixed space-charge tune shift $\Delta\nu_{sc0}$ and the reduced resonance strength $g_{0,4,\ell}$, obtained by varying the betatron amplitude functions at the space-charge kick locations. Extrapolation of each EGF curve with the power law (linear in the log–log plot) back onto the horizontal axis gives us a *critical tune ramp rate*. As an example, the dot-dashed line represents the extrapolation of the EGF of $|g_{0,4,\ell}| = 0.04$. The dot-dashed line cuts the tune ramp rate at $(d\nu/dN)_{\text{critical}} = 0.036$. At the critical tune ramp rate, the EGF is less than 1.2, i.e. the emittance growth is less than 20%. Figure 10 shows the critical tune ramp rate, $(d\nu/dN)_{\text{critical}}$, versus the reduced resonance strength. Given a tune ramp rate, we obtain a tolerable reduced 4th order resonance strength, which provide a guideline for accelerator lattice design.

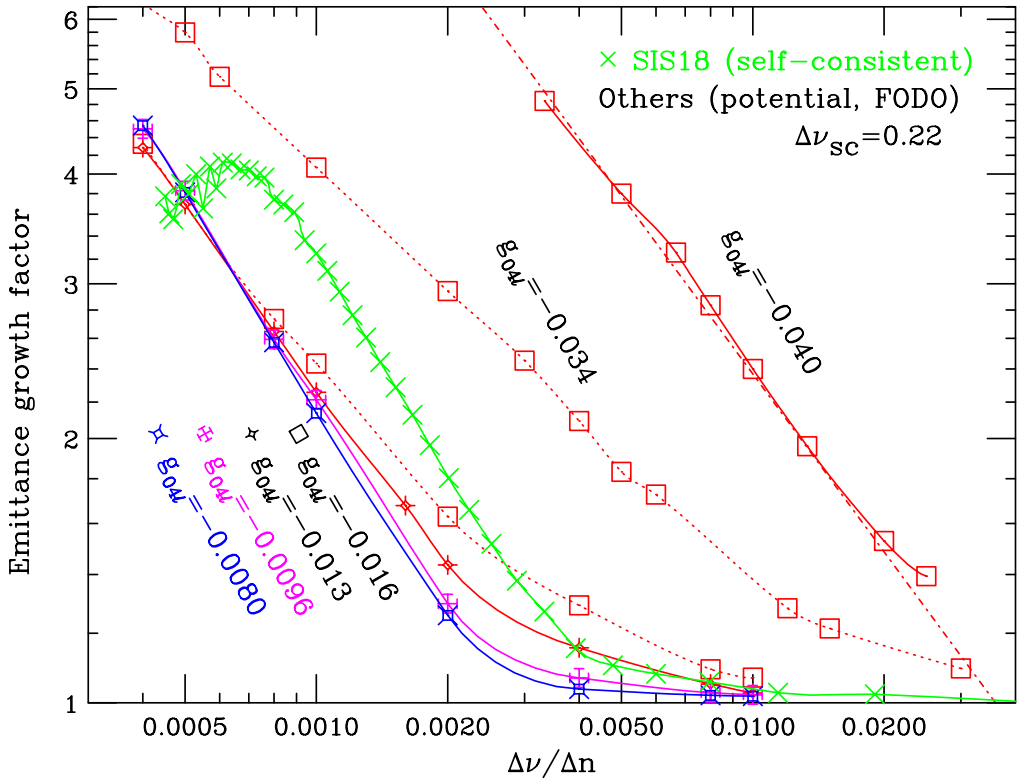

Figure 9. The EGF versus the resonance crossing rate, $\Delta\nu/\Delta n$, through the systematic 4th order space-charge resonance with Laslett space-charge tune shift of 0.22 and various resonance strength $g_{0,4,\ell}$ for the vertical plane. The X-symbols (green) shows the EGF of the SIS18 lattice with similar Laslett tune shift, obtained by a self-consistent space-charge model [7].

4.1. Effect of linear errors

Besides the systematic space-charge resonances, random errors play an important role in particle beam dynamics. Since the dipole field errors affect the closed orbit, which is relevant to the beam emittance at injection, we assume that the closed orbit is properly corrected, and will not discuss this problem further.

The random quadrupoles break the superperiodicity, and produce half-integer stop bands given by equation (14). When the betatron tune of a particle sits on the half-integer stop-band, the action increases exponentially with the number of revolutions. Similarly, the random skew-quadrupoles produces both sum and difference resonances. When the betatron tunes are ramped through many integers, the sum resonance is unavoidable. The stop-band width of a sum resonance is [2]

$$G_{1,1,\ell} = \frac{1}{2\pi}\oint \sqrt{\beta_x(s)\beta_z(s)}A(s)\,\mathrm{e}^{\mathrm{i}[\psi_x(s)+\psi_z(s)-(\nu_x+\nu_z-\ell)s/R]}\,\mathrm{d}s, \tag{16}$$

where $A(s)$ is the skew-quadrupole or solenoidal error field, $\beta_x(s)$ and $\beta_z(s)$ are the horizontal and the vertical betatron amplitude functions, $\psi_x(s)$ and $\psi_z(s)$ are the betatron phase function,

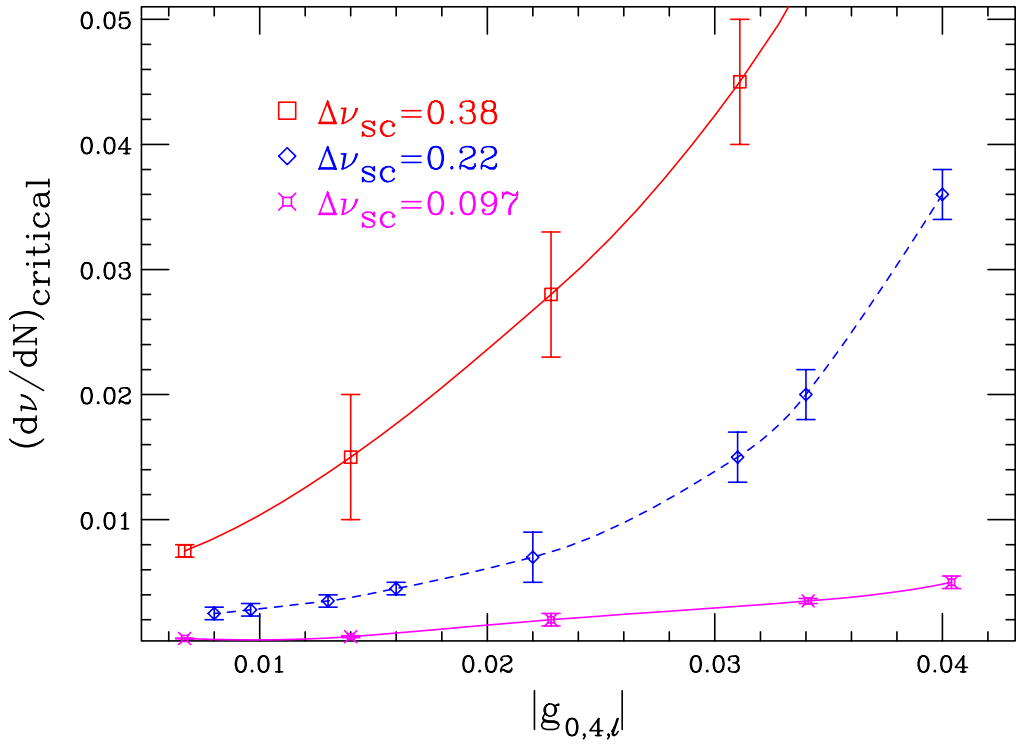

Figure 10. The critical tune ramp rate versus the reduced resonance strength for various space-charge tune shift parameters $\Delta\nu_{sc0}$. The critical tune ramp rate is obtained by extrapolating the EGF curve of figure 8 back to EGF=1 line. At the critical tune ramp rate, the EGF is less than 1.2.

and R is the mean radius of the accelerator. When the betatron tunes of a particle sit on a sum resonance, both the horizontal and vertical actions will grow as $\exp(2\pi|G_{1,1,\ell}|n)$.

Let the stop-band width be $g = |J_p|$ or $g = |G_{1,1,\ell}|$. The EGF in passing through a resonance will be $\exp(2\pi g\Delta n)$, where Δn is the number of revolutions that the tunes of beam particles are inside the stop-band width. Since $\Delta n \sim g/(d\nu/dn)$, we find that the EGF becomes

$$\text{EGF} = \exp\left[\lambda 2\pi g^2/(d\nu/dn)\right], \tag{17}$$

where λ is a constant.

We set up to calculate the EGF induced by the quadrupole and skew-quadrupole error. The algorithm is the same as what we have stated earlier, except that random-quadrupole and skew-quadrupole kicks are added to each half cell [5]. We prepare a beam with $\Delta\nu_{sc0} = 0.217$. The bare betatron tunes are ramped from $(\nu_{x0}, \nu_{z0}) = (6.85, 7.80)$ to $(5.85, 6.80)$ in 50 revolutions. The EGF, resulting from the $4\nu_x = P$ systematic space-charge resonance, is about 1.5 in the horizontal plane.

Now we calculate the EGF for quadrupole and skew-quadrupole errors separately. The quadrupole and skew-quadrupoles are generated by a random number generator. The stop-band width is then calculated from the error seed. Figure 11 shows the EGF as a function of the stop-band width for both the quadrupole error and skew-quadrupole error. We find that the EGF can indeed be described well by $\exp(\lambda 2\pi g^2/(d\nu/dn))$. The EGF for the horizontal plane is dominated

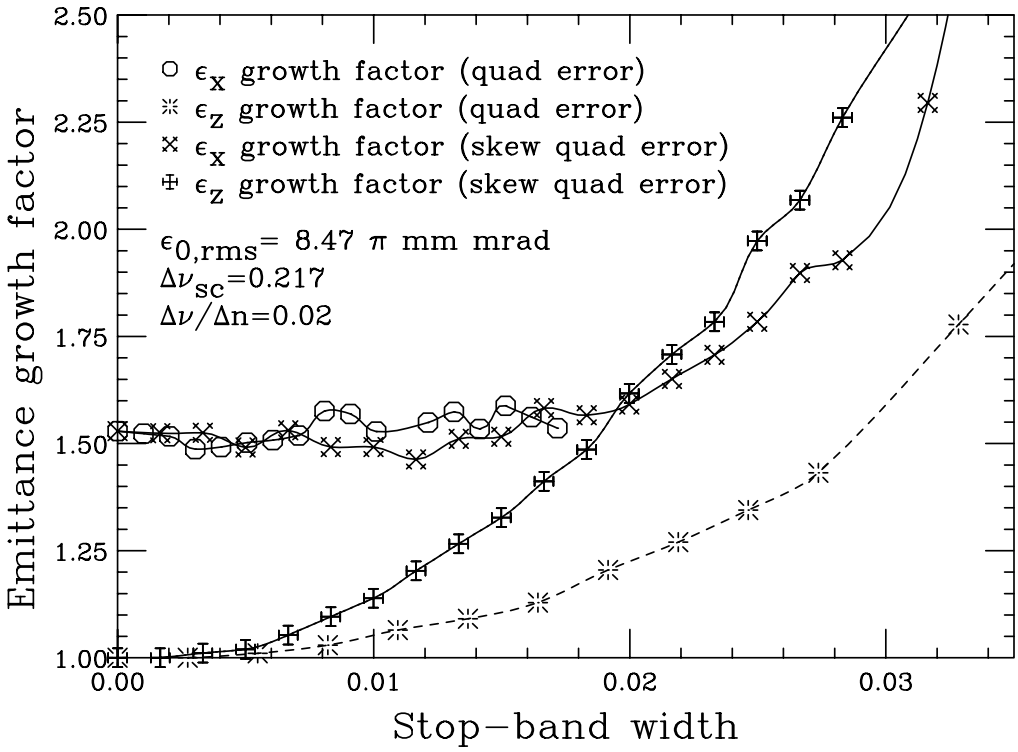

Figure 11. The EGF is plotted as a function of the stop-band width for the random quadrupole and skew-quadrupole errors. The EGF obeys the scaling property: $\exp(\lambda 2\pi g^2/(\mathrm{d}\nu/\mathrm{d}n))$, where λ is a constant, g is the stop-band width, and $\mathrm{d}\nu/\mathrm{d}n$ is the tune ramp rate.

by the crossing of the systematic space-charge resonance at $4\nu_x = P$. Since the vertical tune does not cross the systematic space-charge resonance, its EGF arises solely from the random errors. The random seed used in the quadrupole error happens to produce the stop-band widths (0.017, 0.047) for the horizontal and vertical planes respectively. The ϵ_x growth factor, shown as circle symbols, stops at a stop-band width of about 0.017, because the vertical EGF becomes 3.08 and beam loss occurs.

Figure 12 shows ln(EGF), that arises solely from the random quadrupole and skew-quadrupole errors, as a function of $2\pi g^2/(\mathrm{d}\nu/\mathrm{d}n)$ for $\mathrm{d}\nu/\mathrm{d}n = 0.01$ and 0.02. The scaling property of equation (17) is verified in the numerical simulations. The slope gives $\lambda = 3.5$ for sum resonances, and 1.5 for the half integer stop bands. Data presented in figure 12 include the vertical EGF of figure 11 and other calculations that the effect of systematic space-charge resonance is absence.

5. Conclusion

We use the rms space-charge potential model to study emittance growth mechanisms due to systematic space-charge resonances and random linear errors in accelerators. We find that the systematic space-charge resonance width can be factorized into a geometric factor and a

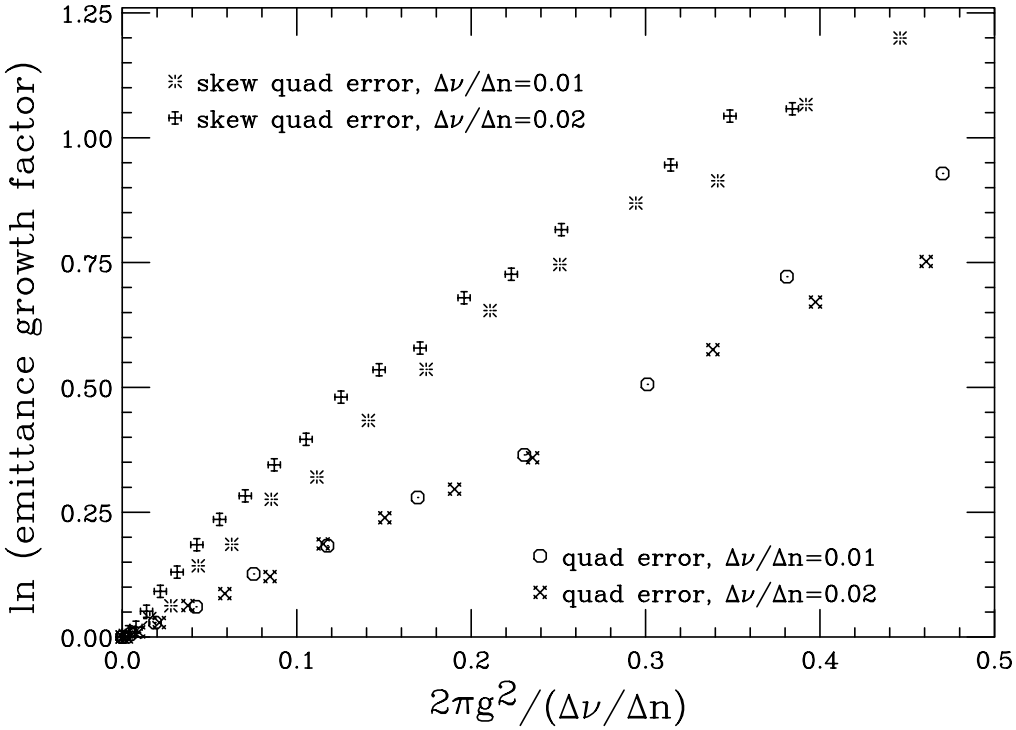

Figure 12. The ln (EGF) is shown as a function of $2\pi g^2/(\mathrm{d}\nu/\mathrm{d}n)$ for random quadrupole and skew-quadrupole errors, where g is the resonance stop-band width, $\mathrm{d}\nu/\mathrm{d}n = 0.01, 0.02$ is the tune ramp rate. The slope is the parameter λ. We find $\lambda \approx 3.5$ for the sum resonances, and 1.5 for the half integer stop bands. Since we are examine the EGF for the random quadrupole and skew-quadrupole errors only, only the EGF data of the vertical plane in figure 11 is used in this plot.

space-charge tune shift. The geometric factor depends essentially on the lattice design. We find that the systematic resonances are important to emittance growth for high intensity proton drivers. It is advisable to design the betatron tunes away from the systematic nonlinear resonances induced by the space-charge potential. However, when the linear errors such as the dipole field errors, quadrupole field errors, and skew-quadrupole field errors are included, emittance growth becomes inevitable. We find that the skew-quadrupole induced sum resonances are important [5]. Stop-band correction for the these resonances is important.

We also carried out the effect of betatron tune ramp through systematic space-charge resonances. We find that the down-ramp causes particularly serious emittance growth because the betatron tunes stay longer at the resonance. We found that the EGF obey power law with the tune ramp rate, i.e. EGF $\sim (\mathrm{d}\nu/\mathrm{d}N)^{-a}$, where $a \approx 0.60 \sim 0.80$. We define a critical tune ramp rate to characterize a tolerable EGF. The critical tune ramp rate was obtained as a function of the reduced 4th order resonance strength $g_{4,0,\ell}$ or $g_{0,4,\ell}$ for various space-charge parameters.

We also study the EGF in tune ramp through linear resonances induced by quadrupole and skew-quadrupole errors. The EGF can be described by a simple scaling law, shown in equation (17) with a ramping rate $\mathrm{d}\nu/\mathrm{d}N \geqslant 0.01$. At a small ramping rate, the space-charge tune shift can enhance the EGF beyond the exponential growth.

Acknowledgments

This study is supported in part by grants from the US Department of Energy under contract DE-FG0292ER40747 and the National Science Foundation NSF PHY-0552389. SYL also thank supports from the Humboldt Foundation in Germany and the Indiana University, USA.

Appendix A. The space-charge potential

One defines the variables:

$$r = \frac{\sigma_z}{\sigma_x}, \qquad a = \frac{x}{\sqrt{2(\sigma_x^2 - \sigma_z^2)}}, \qquad b = \frac{z}{\sqrt{2(\sigma_x^2 - \sigma_z^2)}}, \qquad s^2 = \frac{2\sigma_z^2 + t}{2\sigma_x^2 + t},$$

the space-charge potential of equation (3) becomes

$$V = \frac{2Nr_0}{\gamma} \int_r^1 \frac{1}{1-s^2} \left\{ 1 - \exp\left[-a^2(1-s^2) - b^2 \left(\frac{1}{s^2} - 1 \right) \right] \right\} \mathrm{d}s. \tag{A.1}$$

Changing the dummy variable to $\zeta = as + \mathrm{i}b/s$ with $(r < s < 1)$, we find

$$\Delta x' - j\Delta z' = -\frac{4Nr_0}{\gamma\sqrt{2(\sigma_x^2 - \sigma_z^2)}} \mathrm{e}^{-(a+jb)^2} \int_{ar+j\frac{b}{r}}^{a+jb} \mathrm{e}^{\zeta^2} \mathrm{d}\zeta. \tag{A.2}$$

Using the definition of the complex error function

$$w(z) = \mathrm{e}^{-z^2} \left[1 + \frac{2j}{\sqrt{\pi}} \int_0^z \mathrm{e}^{\zeta^2} \, \mathrm{d}\zeta \right],$$

one obtains

$$\Delta x' - j\Delta z' = \frac{K_{\mathrm{sc}}\ell}{2} \tilde{F}_{\mathrm{sc}}, \tag{A.3}$$

$$\tilde{F}_{\mathrm{sc}} = j\frac{\sqrt{2\pi}}{\sqrt{(\sigma_x^2 - \sigma_z^2)}} \left[w(a+jb) - \mathrm{e}^{-(a+jb)^2 + (ar + j\frac{b}{r})^2} w\left(ar + j\frac{b}{r} \right) \right]. \tag{A.4}$$

The space-charge kick form factors are given by the real and imaginary parts of the form factor $\tilde{F}_{\mathrm{sc}}$, i.e. $\tilde{F}_{x,\mathrm{sc}} = \Re(\tilde{F}_{\mathrm{sc}})$ and $\tilde{F}_{z,\mathrm{sc}} = -\Im(\tilde{F}_{\mathrm{sc}})$. Figure A.1 compares the approximated and the exact form factors at $x = 0.5\sigma_x$ and $1\sigma_x$ as a function of z.

The form factor for the horizontal kicks $F_{x_0,\mathrm{sc}}$ at a nonzero $x_0 = 0.5\sigma_x$ or $1\sigma_x$ value starts at a finite nonzero value as a function of z. The form factor for the vertical kicks $F_{z,\mathrm{sc}}(x_0, z)$ starts from zero. The approximated form factors are good approximation to the exact form factor for $x \leqslant \sigma_x$ and $z \leqslant \sigma_z$. At the large x, z phase space coordinates, i.e. $x > 3\sigma_x$ or $z > 3\sigma_z$, the approximated form factor in equation (4) underestimate the space-charge force.

We also note that the approximated space-charge kicks in equation (4) cannot be derived from a potential, and thus the resulting Montague resonance is only approximately correct. Since this paper focuses on other resonances, the approximated space-charge form factor is

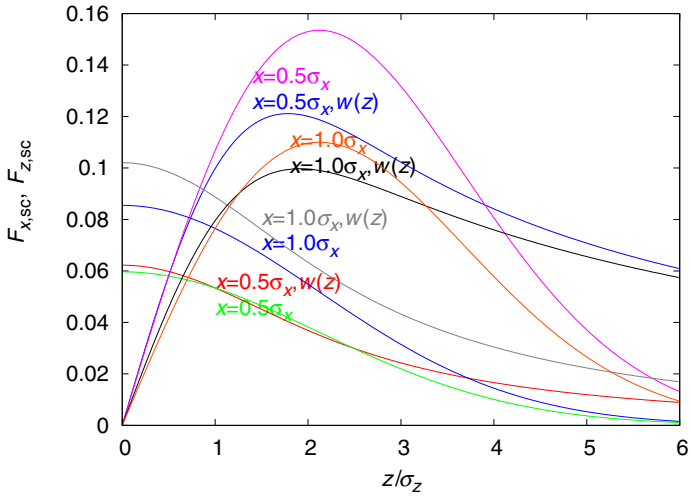

Figure A.1. The approximated space-charge kick form factors of equation (4) is compared with that obtained from the complex error function of equation (A.4) for $\sigma_x = 10\,\text{mm}$, and $\sigma_z = 5\,\text{mm}$ at $x = 0.5\sigma_x$ and $1\sigma_x$ as a function of z. The slope of $\tilde{F}_{z,\text{sc}}$ near $z = 0$ corresponds to the space-charge defocusing quadrupole kick. The form factors $\tilde{F}_{x,\text{sc}}$ are not zero at $z = 0$ because they are evaluated at a finite x values.

usable. In the future, the slightly more time consuming space-charge kicks of equation (A.4) will be implemented in our code, which can read the lattice file directly so that we can carry out space-charge simulations in the accelerator lattice design.

References

[1] Sacherer F J 1968 Transverse space-charge effects in circular accelerators *PhD Thesis* UCRL-18454 (UC Berkeley)
[2] Lee S Y 2004 *Accelerator Physics* 2nd edn (Singapore: World Scientific)
[3] Cousineau S 2002 *PhD Thesis* Indiana University
Cousineau S *et al* 2003 *Phys. Rev. ST Accel. Beams* **6** 034205
[4] Montague B W 1968 CERN-Report No. 68-38
Hofmann I *et al* 2004 *High Intensity and High Brightness Hadron Beams* ed I Hofmann, J M Lagniel and R W Hasse (*AIP Proc. No.* 773) (New York: AIP) p 169
Hofmann I *et al* 2005 *Proc. 2005 Particle Accelerator Conference* (New York: IEEE) p 330
[5] Huang X, Lee S Y, Ng K Y and Su Y 2006 *Phys. Rev. ST Accel. Beams* **9** 014202
[6] Machida S 1994 *Computational Accelerator Physics* ed R Ryne (*AIP Conf. Proc. No.* 297) (New York: AIP) p 459
[7] Bergamini F, Franchetti G and Turchetti G 1999 *Nuovo Cimento* A **112** 429
[8] The Synergia project at Fermilab online at http://cepa.fnal.gov/psm/aas/Advanvced_Accelerator_Simulation.html
[9] Qiang J, Ryne R D, Habib S and Decyk V 2000 *J. Comput. Phys.* **163** 434
[10] Galambos J, Holmes J, Olsen D, Luccio A and Beebe-Wang J 1999 ORBIT user's manual, Oak Ridge National Laboratory, *SNS/ORNL/AP Technical Note No. 011*
[11] Chao A and Month M 1974 *Nucl. Instrum. Methods* **121** 129

[12] Aiba M and Machida S 2004 *Proc. EPAC 2004* (EPAC) p 2119; online at
http://accelconf.web.cern.ch/AccelConf/e04/PAPERS/WEPLT115.PDF
[13] Kheifets S 1976 *PETRA Note 119*
[14] Hofmann I 1981 *Proc. Workshop on the Use of the Spallation Neutron Source for Heavy Ion Fusion Beam Dynamics Studies (Rutherford Laboratories, UK)* p 77
Hofmann I, Franchetti G and Fedotov A 2002 *AIP Conf. Proc.* **642** 248
[15] Igarashi S *et al* 2003 *Proc. PAC 2003* (IEEE), p 2610; online at
http://accelconf.web.cern.ch/AccelConf/p03/PAPERS/WPPG009.PDF
[16] Wang M H and Lee S Y 2002 *J. Appl. Phys.* **92** 555
[17] Berg J S *et al* 2004 *Proc. 17th Cyclotron Conf. Tokyo, Japan* online at
http://accelconf.web.cern.ch/AccelConf/c04/data/CYC2004_papers/19C2.pdf
[18] Ruggiero A 2005 *BNL AP-Technote*: C-A/AP/#219 (BNL)
[19] Hofmann I and Berkert K 1985 *IEEE Trans. Nucl. Sci.* NS- **32** 2264